THE JOURNAL OF BIOLOGICAL CHEMISTRY VOL. 286, NO. 33, pp. 29227–29240, August 19, 2011

Site-1 Protease Is Essential to Growth Plate Maintenance and Is a Critical Regulator of Chondrocyte Hypertrophic Differentiation in Postnatal Mice*[S]

Received for publication, December 2, 2010, and in revised form, May 6, 2011 Published, JBC Papers in Press, June 7, 2011, DOI 10.1074/jbc.M110.208686

Debabrata Patra[‡1], **Elizabeth DeLassus**[‡], **Shinya Hayashi**[‡], **and Linda J. Sandell**[‡§2]

From the Departments of [‡]*Orthopaedic Surgery and* [§]*Cell Biology and Physiology, Washington University School of Medicine at Barnes-Jewish Hospital, St. Louis, Missouri 63110*

Site-1 protease (S1P) is a proprotein convertase with essential functions in lipid homeostasis and unfolded protein response pathways. We previously studied a mouse model of cartilage-specific knock-out of S1P in chondroprogenitor cells. These mice exhibited a defective cartilage matrix devoid of type II collagen protein (Col II) and displayed chondrodysplasia with no endochondral bone formation even though the molecular program for endochondral bone development appeared intact. To gain insights into S1P function, we generated and studied a mouse model in which S1P is ablated in postnatal chondrocytes. Postnatal ablation of S1P results in chondrodysplasia. However, unlike early embryonic ablations, the growth plates of these mice exhibit a lack of *Ihh*, *PTHrP-R*, and *Col10* expression indicating a loss of chondrocyte hypertrophic differentiation and thus disruption of the molecular program required for endochondral bone development. S1P ablation results in rapid growth plate disruption due to intracellular Col II entrapment concomitant with loss of chondrocyte hypertrophy suggesting that these two processes are related. Entrapment of Col II in the chondrocytes of the prospective secondary ossification center precludes its development. Trabecular bone formation is dramatically diminished in the primary spongiosa and is eventually lost. The primary growth plate is eradicated by apoptosis but is gradually replaced by a fully functional new growth plate from progenitor stem cells capable of supporting new bone growth. Our study thus demonstrates that S1P has fundamental roles in the preservation of postnatal growth plate through chondrocyte differentiation and Col II deposition and functions to couple growth plate maturation to trabecular bone development in growing mice.

Site-1 protease (S1P[3]; also known as the membrane-bound transcription factor protease, site-1) is a proprotein convertase that plays a vital role in maintaining lipid homeostasis and unfolded protein response through regulated intramembrane proteolysis pathways. During lipid homeostasis, S1P is involved in the proteolytic maturation of the latent endoplasmic reticulum membrane-bound sterol regulatory element-binding protein transcription factors that direct the synthesis of proteins involved in cholesterol and fatty acid synthesis and uptake (1, 2). During unfolded protein response, S1P is involved in the maturation of the endoplasmic reticulum membrane-bound transcription factors ATF6 (3), old astrocyte specifically induced substance (4), and cAMP-responsive element-binding protein H (5).

Several recent studies have also implicated a role for S1P in skeletal development, although the exact molecular nature of this requirement is not known. Mammalian skeletal development takes place largely through the process of endochondral ossification in which mesenchymal cell condensates differentiate to form chondrocytes. Chondrocytes secrete the type II collagen (Col II)-rich cartilaginous anlagen to form a template for the development of the skeletal structural elements (6). This process involves the differentiation of the central-most chondrocytes into hypertrophic chondrocytes that secrete a type X collagen (Col X)-rich matrix that becomes calcified. The vascular invasion of this matrix from the surrounding bone collar and the entry of osteoclasts and osteoblasts that degrade the Col X-rich matrix initiate replacement of the cartilage by bone. Removal of the hypertrophic cells by apoptosis and the deposition of the type I collagen-rich bone matrix by the osteoblasts result in bone growth toward both bone ends. A continuous cycle of chondrocyte hypertrophic differentiation in the newly formed growth plate allows for continuous bone deposition and therefore bone elongation. Thus, hypertrophic chondrocyte differentiation is fundamental to the endochondral bone developmental program.

In zebrafish, ablation of S1P activity results in abnormal cartilage development and an accumulation of both lipid and skeletal abnormalities (7). We have shown that S1P is essential to endochondral bone development as cartilage-specific ablation of S1P activity in mice ($S1P^{cko}$) results in severe chondrodysplasia (8). $S1P^{cko}$ mice do not form any endochondral bone. This defect may be due to the abnormal cartilage deposition in these mice as the Col II protein is largely trapped inside the cell with consequent reduction of Col II in the cartilaginous matrix. As $S1P^{cko}$ mice die during or shortly after birth, the study was restricted to embryonic time points. Given the profound carti-

* This work was supported, in whole or in part, by National Institutes of Health Grants RO1 AR050847 and RO1 AR045550 (to L. J. S.) and by Grant P30 AR057235 to the Washington University Center for Musculoskeletal Research.

[S] The on-line version of this article (available at http://www.jbc.org) contains supplemental Figs. 1–12 and Table 1.

[1] To whom correspondence may be addressed: Dept. of Orthopaedic Surgery, Washington University School of Medicine at Barnes-Jewish Hospital, 660 S. Euclid Ave., Box 8233, St. Louis, MO 63110. Fax: 314-454-5900; E-mail: patrad@wudosis.wustl.edu.

[2] To whom correspondence may be addressed. E-mail: sandelll@wustl.edu.

[3] The abbreviations used are: S1P, site-1 protease; Col II, type II collagen protein; Col X, type X collagen protein; ISH, *in situ* hybridization; PTHrP-R, parathyroid hormone related peptide-receptor; μCT, microCT; SOC, secondary ossification center; TRITC, tetramethylrhodamine isothiocyanate; BV/TV, bone volume/total volume; BMD, bone mineral density.

lage and loss of bone phenotype in S1P^{cko} mice, we wanted to investigate the requirement for S1P in chondrocytes of the postnatal growth plate. Therefore, to gain insights into the nature of S1P function, we have used the Col2CreER^{T} mice (9) that allowed us to abolish S1P activity in postnatal mice through tamoxifen administration in a temporal manner. Our study shows that the removal of S1P activity in postnatal mice results in loss of chondrocyte hypertrophic differentiation in parallel with Col II retention in the cell and the eventual loss of the growth plate through apoptosis. The consequent chondrodysplasia and loss of trabecular development in the long bones of the body underscore the fundamental need for S1P in maintaining skeletal homeostasis throughout postnatal development.

EXPERIMENTAL PROCEDURES

Generation of S1P$^{cko\text{-}ER(T)}$ Mice—To generate S1P$^{cko\text{-}ER(T)}$ mice, S1P$^{f/f}$ mice (mice homozygous for the S1P^{flox} allele, where S1P exon 2 is floxed (10)) were bred with Col2CreER^{T} mice (mice in which the Cre recombinase is directed by the cartilage-specific *Col2a1* promoter limiting its expression primarily to cartilage and is also tamoxifen-dependent requiring tamoxifen injections for Cre recombinase activity (9)) to produce S1P$^{f/+}$; Col2CreER^{T} mice (mice heterozygous for the S1P^{flox} allele and positive for the Col2-CreER^{T} transgene). S1P$^{f/+}$;Col2CreER^{T} mice were mated with each other to produce S1P$^{f/f}$; Col2CreER^{T} mice that demonstrated wild type (WT) characteristics in the absence of tamoxifen. S1P$^{f/f}$ mice were bred with S1P$^{f/f}$;Col2CreER^{T} mice and neonatal mice or pregnant females were injected with tamoxifen. All WT controls are S1P$^{f/f}$ mice. After tamoxifen administration, S1P$^{f/f}$;Col2CreER^{T} mice are referred to as S1P$^{cko\text{-}ER(T)}$ mice. In the absence of tamoxifen, no leaky recombination was observed as evidenced by the lack of lethality in newborn mice or by the absence of bone phenotype/chondrodysplasia in adult mice indicating a tightly controlled tamoxifen and Cre-dependent removal of S1P activity.

Tamoxifen Injections and Harvesting of Mice—For ease of mixing and administration, tamoxifen (Sigma) was dissolved in 100% ethanol (500 mg/ml) to which was added corn oil to give a final concentration of 20 mg/ml. Pregnant female mice from crosses of S1P$^{f/f}$ and S1P$^{f/f}$;Col2CreER^{T} mice were given a single dose of 3 mg of tamoxifen at 10.5 or 13.5 days postcoitus and harvested at embryonic (E) stage 18.5 to give E10.5–E18.5 and E13.5–E18.5 S1P$^{cko\text{-}ER(T)}$ mice, respectively. Newborn mouse pups (P1), both S1P$^{f/f}$ (WT) and S1P$^{f/f}$;Col2CreER^{T}, were injected with 1 mg of tamoxifen suspension in corn oil and harvested when 3, 5, 7, or 14 days old and are referred to as P1–P3, P1–P5, P1–P7, or P1–P14 WT and S1P$^{cko\text{-}ER(T)}$ mice, respectively. P7 mice were given a dose of 100 μg/g of body weight and were harvested when P15, P28, or P42 and are referred to as P7–P15, P7–P28, or P7–P42 WT and S1P$^{cko\text{-}ER(T)}$ mice, respectively. To avoid difficulty and complications involved with injecting P1 pups, pregnant females were tested by injecting at E18.5 gestation stage, and the pups were harvested when 14 days old to give E18.5–P14 S1P$^{cko\text{-}ER(T)}$ mice. Fig. 1 summarizes the temporal design of S1P ablations and analysis.

MicroCT (μCT) Analysis—For micro-computed tomography (μCT) analyses, the mice were skinned, eviscerated, and fixed in 10% neutral buffered formalin for 24–48 h, followed by washing with phosphate-buffered saline and storage in 70% ethanol until scanning. Femurs and humeri were separated from the mouse body, stripped of muscle tissues, and scanned. All scans were done in a MicroCT 40 scanner (Scanco Medical AG, Switzerland) under high resolution at tube settings of 55-kV peak energy, 145 μA of current with an integration time of 150 ms in a tube of diameter 16.4 mm. Segmentation was done to distinguish high density (bone) from low density (soft tissue/cartilage/growth plate) areas. Images from individual scan slices or reconstructed bones were captured as TIFF images. Histomorphometric measurements of bone volume fraction (BV/TV) and bone mineral density (BMD) (expressed as milligrams of hydroxyapatite/cm^3) were calculated using 50 scan slices beginning from the metaphyseal side of the chondro-osseous junction (see Fig. 8*A*), using the manufacturer's three-dimensional analysis tools and are based on the direct method of calculation (11).

Morphological and Histological Analyses—Histological analyses by Safranin O, Fast Green, and hematoxylin staining were done on formalin-fixed, paraffin-embedded tissues cut 5 μm thick. Tissues E18.5 and older were decalcified with 14% free acid EDTA (pH adjusted to 7.2 with ammonium hydroxide) until soft to cut. Tartrate-resistant acid phosphatase-positive cells were stained using standard procedures with hematoxylin as counterstain. *In situ* hybridization (ISH) analyses with ^{35}S-labeled probes were done as described previously (8, 12). Apoptosis of chondrocytes was analyzed by a TUNEL assay using the *in situ* cell death detection kit (Roche Applied Science) according to the manufacturer's instructions with nuclei counterstained by DAPI. Detection of Col II protein by immunohistochemistry was done on hyaluronidase (1% for 30 min at 37 °C)- treated paraffin-embedded tissues using the IIF antibody described previously (8, 13) with HRP-conjugated goat-anti-rat secondary antibody and a DAB substrate (Invitrogen) with tartrazine as counterstain. Double-labeled immunofluorescence with IIF and IIA antibodies was performed as described previously (8, 13) on hyaluronidase or proteinase K (10 μg/ml in 10 mM Tris-HCl, pH 7.5, for 20 min at 37 °C) treated paraffin-embedded tissues with the exception that both primary (or secondary) antibodies were added simultaneously rather than sequentially. The images were captured using a 60X, 1.4 NA oil immersion objective mounted on an Eclipse E800 microscope (Nikon) and QImaging Retiga 2000R Fast 1394 camera and Eclipse 5.0 (Empix Imaging) software. ISH images or histological images were viewed with BX51 (Olympus) microscope and images captured with a digital camera (DP70; Olympus) using DP controller software (Olympus). Pictures of hybridization signals were artificially colored red and superimposed on toluidine blue-counterstained images using Photoshop (Adobe). To label new cortical bone formation, P7–P28 mice were injected with the fluorochromes calcein green (Sigma; 10 mg/kg given intraperitoneally) on day 21 and alizarin complexone (Sigma; 30 mg/kg given intraperitoneally) on day 26 and harvested on day 28 by CO_2 asphyxiation. The femurs and humeri were fixed in 10% formalin for 24–48 h, dehydrated, and embedded in methyl methacrylate (14), and 50-μm thick sections were cut, mounted on glass slides, and

visualized for incorporation of calcein (FITC filter) and alizarin (TRITC filter) by fluorescent microscopy (Olympus BX51), and images were digitized and merged (Olympus DP70).

RESULTS

S1P Ablations at E10.5 and E13.5 Results in Chondrodysplasia in S1P$^{cko\text{-}ER(T)}$ Mice—To analyze loss of S1P activity with the Col2CreER^{T} system, S1P$^{f/f}$ mice were mated with S1P$^{f/f}$; Col2CreER^{T} mice, and tamoxifen was administered. Fig. 1 summarizes the temporal design of tamoxifen administrations and analyses. Table 1 summarizes some key phenotypic manifestations of S1P ablations and the differences between pre- and postnatal ablations. To first analyze that Col2CreER^{T} mice do indeed cause loss of S1P activity on tamoxifen administration, we injected tamoxifen into pregnant mothers at 10.5 and 13.5 days post-coitus to test if this results in chondrodysplasia and lack of endochondral bone as seen in the S1P^{cko} (S1P$^{f/f}$; Col2Cre) mice (8). Mice were harvested and analyzed at E18.5. Tamoxifen administration at both E10.5 and E13.5 resulted in chondrodysplasia (data not shown), loss of endochondral bone (see below), and in fatality during or very soon after birth. Furthermore, ISH analyses demonstrated the loss of S1P in the cartilage of both E10.5–E18.5 and E13.5–E18.5 S1P$^{cko\text{-}ER(T)}$ mice indicating that the use of Col2CreER^{T} system successfully eliminated S1P expression (supplemental Fig. S1) and that the resulting phenotype is due to loss of S1P activity.

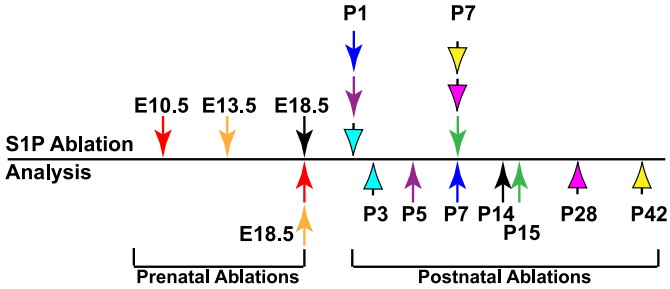

FIGURE 1. **Line drawing showing the timing of tamoxifen administrations for S1P ablation in pre- and postnatal S1P$^{f/f}$ and S1P$^{f/f}$;Col2CreER^{T} mice and harvesting of mice for analysis.** Prenatal ablations were accomplished by tamoxifen administration to the pregnant females at 10.5, 13.5, or 18.5 days postcoitus. *Arrows above* the line point to the time when S1P was ablated. A like-colored *arrow below* the line points to the time when the corresponding mice were harvested for analysis. For example, the *green arrows* demonstrate that postnatal mice with S1P ablation at P7 were harvested at P15 (P7–P15 WT or S1P$^{cko\text{-}ER(T)}$ mice) for analysis.

Notably, S1P ablation at E10.5 (Fig. 2) resulted in a complete loss of endochondral bone formation along with the presence of an enhanced cortical bone formation (Fig. 2*B*, *arrow*), thus phenocopying the S1P^{cko} mice. Like the S1P^{cko} mice, ISH analyses demonstrated expression of *Ihh* (*indian hedgehog*; Fig. 2*F*), *PTHrP-R* (*parathyroid hormone related peptide-receptor*; Fig. 2*H*), and *Col10* (Fig. 2*J*) suggesting that the molecular program needed for hypertrophic differentiation and endochondral bone development is intact in these mice. S1P$^{cko\text{-}ER(T)}$ mice also demonstrated an increased chondrocyte apoptosis (Fig. 2*L*). To analyze if S1P ablation at E10.5 results in an abnormal Col II phenotype, we performed double-labeled immunofluorescence for the Col IIA protein using the IIA antibody (specific for Col II exon 2; localizations are shown in *green*) and the IIF antibody (specific for Col II triple helical domain; localizations are shown in *red*) (Fig. 3). This helps to distinguish the distribution of Col IIB, which is the chondrocyte-specific Col II, from its splice variant Col IIA, which is chondroprogenitor-derived. In WT, in the matrix surrounding the early reserve chondrocytes, Col IIA in the matrix is seen as a well organized green lattice network that is distinct from the red lattice network of the Col II triple helical domain (Fig. 3*A*). As chondrocytes make primarily Col IIB, which does not have exon2-specific amino acids, the lack of any colocalization signals from the two antibodies suggest that the red lattice network represents primarily Col IIB. In the mutant, only a distinct green lattice network for Col IIA is seen in the cartilage (Fig. 3, *B* and *C*). A red lattice network for Col IIB is absent. Col IIB is seen primarily trapped inside the cell (*arrow,* Fig. 3*C*), as in the S1P^{cko} mice.

In WT around the mature columnar chondrocytes (Fig. 3, *D* and *G*), strong signaling from Col IIB protein (*red*) is seen especially in the pericellular matrix (*arrowheads*) and very little Col IIA matrix (*green*). In E10.5–E18.5 S1P$^{cko\text{-}ER(T)}$ mice, in a corresponding region surrounding mature chondrocytes, a mixed phenotype is seen (Fig. 3, *E, F, H,* and *I*). A phenotype similar to WT showing the presence of Col IIB (in *red*)-derived pericellular matrix (*arrowheads*, Fig. 3*H*) is seen. Yet there are predominantly Col IIA-rich regions in the matrix (Fig. 3*F*) showing intracellular Col IIB retention (*arrows,* Fig. 3*I*). Around the hypertrophic cells in the WT (Fig. 3, *J* and *M*) a well formed, structurally intact matrix is seen without any retention of Col II intracellularly. The mutant matrix, however, is still predominantly Col IIA-rich seen as a distinct green lattice (Fig. 3, *K, L, N,*

TABLE 1
A summary of similarities and differences in the mutant phenotypes from pre- and postnatal S1P ablations

Ablations	Expression of			Intracellular retention of Col II	Chondrocyte apoptosis	Endochondral bone formation
	Col10	*Ihh*	*PTHrP-R*			
Prenatal						
S1P^{cko} (8)	Yes	Yes	Yes	Yes	Yes	Absent
E10.5–E18.5	Yes	Yes	Yes	Yes; similar to S1P^{cko}	Yes	Absent
E13.5–E18.5	Yes	Yes	Yes	Yes; similar to S1P^{cko}	Yes	Partial development
E18.5–P14	No	No	No	Yes	Yes	Bone sclerotic with drastically diminished trabecular bone; no SOC development; additional growth plate development
Postnatal						
P1–P7	No	No	No	Yes	Yes	Bone sclerotic with drastically diminished trabecular bone; no SOC development
P1–P14	No	No	No	Yes	Yes	Bone sclerotic with drastically diminished trabecular bone; no SOC development; additional growth plate development
P7–P15	No	No	No	Yes	Yes	Bone sclerotic with drastically diminished trabecular bone; additional growth plate development

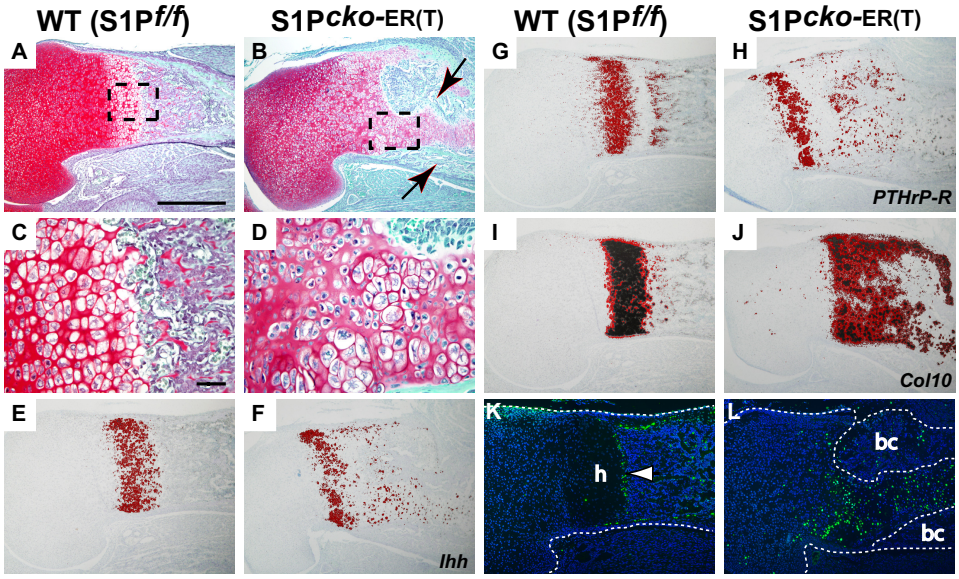

FIGURE 2. **S1P ablation at E10.5 phenocopies the S1P^{cko} mice.** Safranin O/Fast Green-stained sections of the proximal humerus of E10.5–E18.5 WT (S1P$^{f/f}$) (*A* and *C*) and S1P$^{cko\text{-}ER(T)}$ (*B* and *D*) mice are shown. *C* and *D* are higher magnification images of *A* and *B*, respectively, with the areas magnified *outlined*. Panels show the lack of endochondral bone (*B*), the presence of the exuberant bone collar (*arrows* in *B*), and the lack of an organized hypertrophic zone (*D*) in the S1P$^{cko\text{-}ER(T)}$ mice, similar to that seen in the S1P^{cko} mice. ISH analyses in the proximal humeri for *Ihh* (*E* and *F*), *PTHrP-R* (*G* and *H*), and *Col10* (*I* and *J*) show their expression in the mutant growth plate. TUNEL assays (*K* and *L*) in the humeri show increased apoptosis in the mutant cartilage (*h,* hypertrophic cells; *bc,* bone collar). *Bars, A, B,* and *E–J,* 500 μm; *C* and *D,* 50 μm; *K* and *L,* 200 μm.

and *O*) in the hypertrophic region. Col IIB is seen as either trapped inside the cell (*arrows* in Fig. 3*O*) or as secreted but is unable to form a structurally stable matrix (Fig. 3, *K* and *N*). In the latter, Col IIB in the matrix is observed largely as abnormal polygonal "ring-like" structures that could be a visualization of a collapsing Col II matrix unable to retain its structural integrity and shape.

S1P ablation at E13.5 showed a mixed phenotype (supplemental Fig. S2). E13.5–E18.5 S1P$^{cko\text{-}ER(T)}$ mice show an enhanced cortical bone (*arrow,* supplemental Fig. S2*B*) and endochondral bone formation (*arrowhead,* supplemental Fig. S2, *B* and *D*). But the endochondral bone is incipient and never develops completely. Chondrocytes are randomly organized in the growth plate as opposed to the columnar organization seen in the WT. ISH analyses confirmed the presence of *Ihh*-, *PTHrP-R*-, and *Col10*-expressing cells (supplemental Fig. S2, *E–J*) suggesting the preservation of the molecular program required for hypertrophic differentiation and endochondral bone development. TUNEL assays also demonstrated increased chondrocyte apoptosis in the cartilage (supplemental Fig. S2, *K* and *L*). Deposition of the Col II protein was also analyzed by double-labeled immunofluorescence studies (supplemental Fig. S3) using the IIA and IIF antibodies. As in the E10.5–E18.5 S1P$^{cko\text{-}ER(T)}$ mice, the cartilage matrix in E13.5–E18.5 S1P$^{cko\text{-}ER(T)}$ mice was largely dominated by Col IIA protein with the Col IIB trapped inside the cell (supplemental Fig. S3, *B, C, E,* and *H*). Like the E10.5–E18.5 S1P$^{cko\text{-}ER(T)}$ mice, the matrix surrounding mature chondrocytes (supplemental Fig. S3, *F, I, K,* and *L*) was characterized by the inability of the mutant to stabilize Col II in the matrix as interpreted from the unusual ring-like structures of Col IIB in the matrix. In summary, the use of the Col2CreER^{T} system therefore demonstrated successful ablation of S1P activity in these mice.

S1P Ablations in Postnatal Mice Results in Abolition of Chondrocyte Hypertrophic Differentiation—The Col2CreER^{T} mice resulted in successful S1P ablation in the prenatal mice as described above. Therefore, we next utilized the Col2CreER^{T} system to ablate S1P in postnatal mice. The study of postnatal mice also offered the opportunity to examine the development of the secondary ossification center (SOC). First, we analyzed S1P ablation in newborn (P1) mice and analyzed endochondral bone development at P7 or P14 (Fig. 4). Interestingly, unlike S1P^{cko} or the prenatal ablations, S1P ablation in postnatal mice disrupted the molecular program fundamental to endochondral bone growth. Both P1–P7 (Fig. 4, *B, D, F,* and *H*) and P1–P14 (Fig. 4*P*) S1P$^{cko\text{-}ER(T)}$ mice showed disruption of the growth plate, namely the absence of chondrocyte maturation to hypertrophic differentiation. Tamoxifen administration into WT pups (Fig. 4, *A, C, E, G,* and *O*) did not show any phenotype. As chondrocyte hypertrophy in the growth plate is well established by the E15 gestation stage, these data indicated that removal of S1P activity postnatally prevented further hypertrophic differentiation, even though other aspects of the growth plate such as the presence of reserve chondrocytes and the columnar organization of chondrocytes are not affected. ISH analyses confirmed the lack of *Col10* expression in the mutant growth plate (Fig. 4*N*). Expression of *Ihh* (Fig. 4*J*) and *PTHrP-R* (Fig. 4*L*), normally expressed in the prehypertrophic chondrocytes in the primary growth plate, is also missing. In the WT development of the prospective SOC is evidenced through the hypertrophic differentiation of the chondrocytes showing *Col10* expression (*arrow,* Fig. 4*M*). However, *Col10* expression is absent in the corresponding region in the mutant mice indicating disruption of SOC development (Fig. 4*N*). Consequently, no SOC development is seen in P1–P14 S1P$^{cko\text{-}ER(T)}$ mice (Fig.

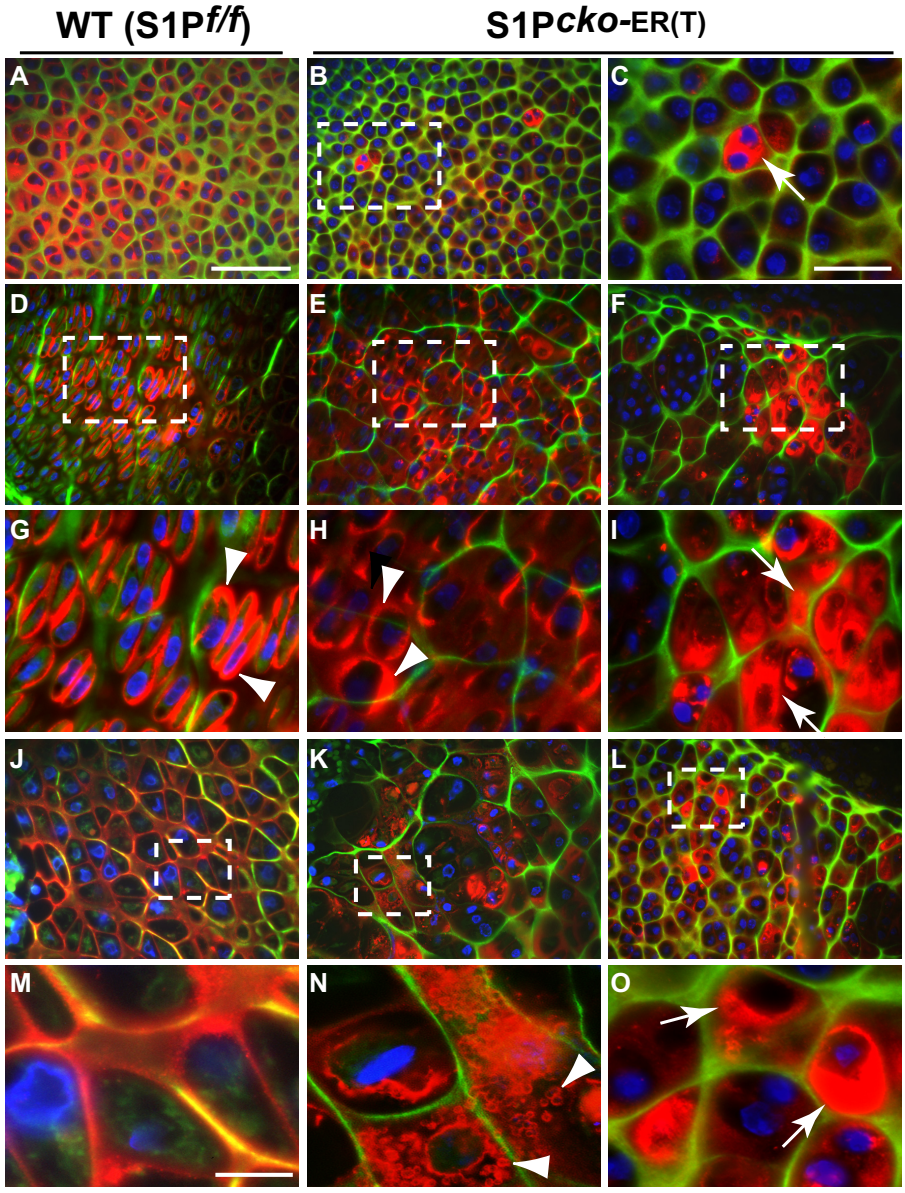

FIGURE 3. **Abnormal Col II deposition in the humeri of E10.5–E18.5 S1P$^{cko\text{-}ER(T)}$ mice.** Double-labeled immunofluorescence studies with IIF and IIA antibodies in the humerus of E10.5–E18.5 WT (S1P$^{f/f}$) and S1P$^{cko\text{-}ER(T)}$ mice showing abnormal Col II (interpreted as primarily Col IIB; see text) distribution in the mutant. *C* is a higher magnification image of *B*; *G–I* are higher magnification images of *D–F*, respectively; *M–O* are higher magnification images of *J–L*, respectively. Areas magnified have been *outlined* in the panels. *A–C* show Col II deposition around early immature chondrocytes; *D–F* show Col II deposition around the proliferative columnar chondrocytes; *J–L* show the hypertrophic zone. *E, F, K,* and *L* show two different regions of columnar and hypertrophic cells, showing the mixed Col IIB phenotype in the mutant. Colors represent antibody localizations as follows: *green*, Col II exon 2 (IIA); *red*, Col II triple helical domain (IIF); *yellow*, colocalization of both antibodies; *blue*, DAPI-stained nuclei. *Arrows* in *C, I,* and *O* point to the entrapment of Col IIB inside the cell; *arrowheads* point to the deposition of Col IIB in the pericellular matrix (*G* and *H*) or to the ring-like Col IIB anomaly in the cartilage (*N*) suggesting a loss of Col IIB integrity in the mutant matrix. *Bars, A, B, D–F,* and *J–L,* 50 μm; *C* and *G–I,* 20 μm; *M–O,* 10 μm.

4*P*). These data suggested that S1P is essential to preserving the growth plate in postnatal mice.

To understand the Col II phenotype in these mice, we performed immunohistochemistry for Col II using the IIF antibody, which detects total Col II (Col IIA plus Col IIB), in P1–P7 mice (Fig. 5). In WT mice, Col II (in *brown*) is detected primarily in the matrix (Fig. 5, *A* and *E*) and as a ring of Col II in the pericellular matrix of the hypertrophic cells in the prospective SOC (Fig. 5, *A, C, E,* and *G*). However, in P1–P7 and P1–P14 (data not shown) mutants, although Col II is detected in the matrix, abnormal retention of Col II is seen inside the chondrocytes (Fig. 5, *B, D, F,* and *H*) in the prospective SOC. As shown in Fig. 4 above, P1–P7 mutants lack *Col10*-expressing cells and the beginnings of an SOC. Thus, the retention of Col II inside the cell marks the disruption of normal SOC development in this region. To understand the distribution of Col IIB in the SOC, double-labeled immunofluorescence using the IIA and IIF antibodies were performed as above (Fig. 5, *I–P*). The WT matrix is characterized by a predominantly Col IIB matrix with strong deposition of Col IIB seen in the pericellular matrix (Fig. 5, *K* and *O*) and at times colocalization of Col IIA and Col IIB signals (*yellow*). No intracellular retention of Col IIB is seen. In the mutant P1–P7 (Fig. 5, *J, L, N,* and *P*), however, the matrix is marked by a Col IIA (*green*) lattice network, with Col IIB (*red*)

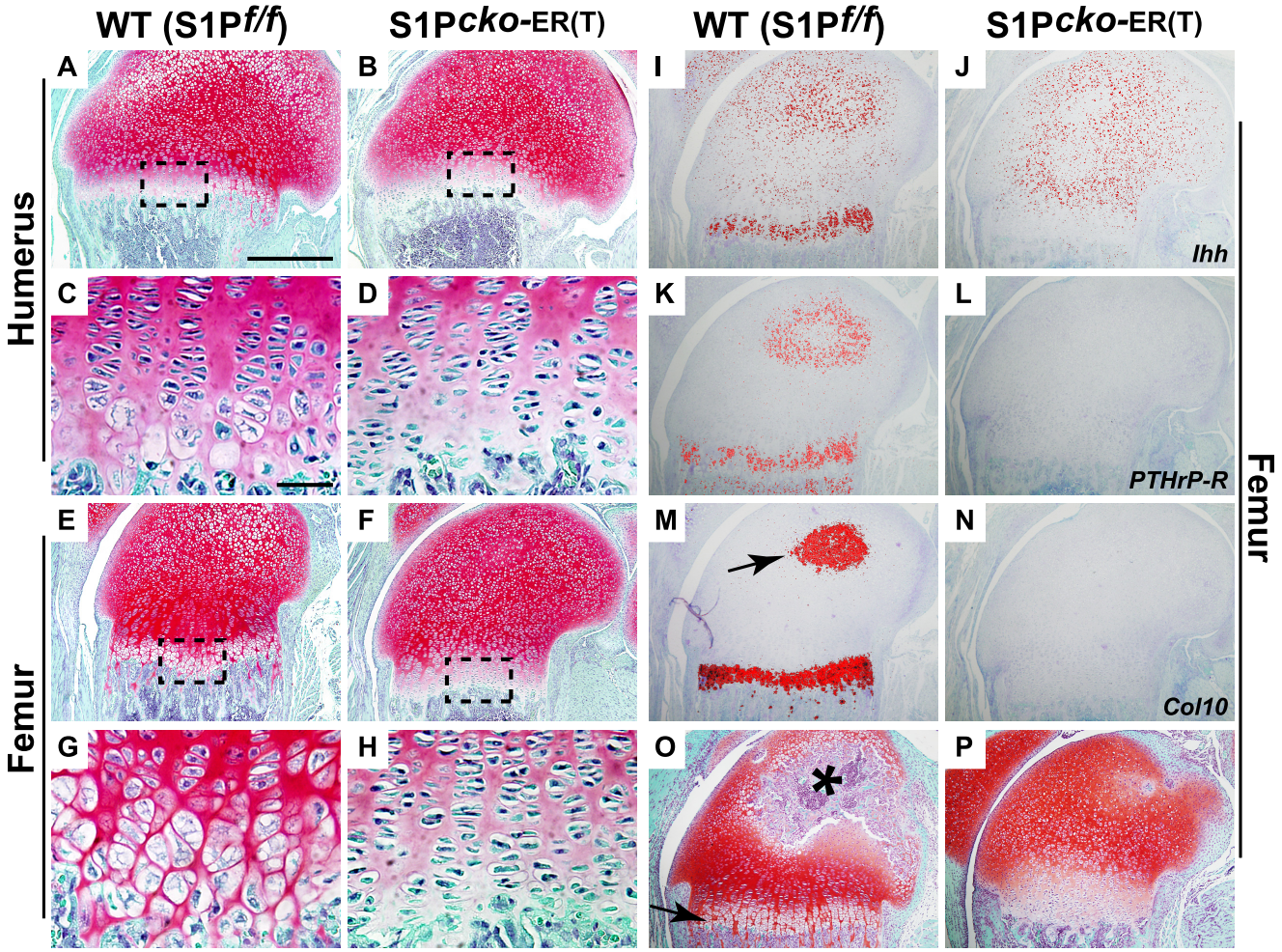

FIGURE 4. **Loss of hypertrophic differentiation on S1P ablation in P1 mice.** Safranin O/Fast Green-stained sections of WT (S1P$^{f/f}$) and S1P$^{cko\text{-}ER(T)}$ humeri (*A–D*) and femurs (*E–H*) showing the disruption of chondrocyte hypertrophic differentiation on S1P ablation in P1–P7 S1P$^{cko\text{-}ER(T)}$ (*B, D, F,* and *H*) humerus/femur as compared with the WT (*A, C, E,* and *G*). ISH analyses in the femur for *Ihh* (*I* and *J*), *PTHrP-R* (*K* and *L*), and *Col10* (*M* and *N*) genes in P1–P7 mice confirm the loss of hypertrophic differentiation in the mutant mice. *Arrow* in *M* points to *Col10* expression in the prospective SOC in the WT. Safranin O/Fast Green-stained sections of P1–P14 WT (*O*) and S1P$^{cko\text{-}ER(T)}$ (*P*) femur showing the presence of hypertrophic cells in the WT (*arrow*) and the formation of SOC (*asterisk*), both notably absent in the mutant. *Bars, A, B, E, F,* and *I–P,* 500 μm; *C, D, G,* and *H,* 50 μm.

retained primarily inside the cells (*arrows,* Fig. 5, *L* and *P*). Intracellular retention is, however, notably decreased in chondrocytes of the growth plate presumably because of chondrocyte clearing by apoptosis (data not shown; also see Fig. 7 and supplemental Fig. S6). Thus, the intracellular Col IIB retention characteristic of S1P loss is also seen in postnatal ablations and in the SOC.

S1P ablations were also performed in P7 mice and analyzed at P15 (P7–P15 WT and S1P$^{cko\text{-}ER(T)}$ mice; Fig. 6). As in the P1–P7 S1P$^{cko\text{-}ER(T)}$ mice, the growth plate in P7–P15 S1P$^{cko\text{-}ER(T)}$ mice is marked by the absence of hypertrophic cells in both the humerus (Fig. 6, *B* and *D*) and femur (Fig. 6, *F* and *H*), although the columnar arrangement of the chondrocytes and organization of the reserve chondrocytes are not disrupted. The growth plate is characterized by the absence of *Ihh* (Fig. 6*J*), *PTHrP-R* (Fig. 6*L*), and *Col10* (Fig. 6*N*) expression indicating a cessation of hypertrophic differentiation on S1P ablation. Double-labeled immunofluorescence with IIA and IIF antibodies demonstrated the intracellular retention of Col IIB in cells of the SOC (data not shown) and in the growth plate (Fig. 6*P*). We also performed S1P ablations at E18.5 while *in utero*. Although this is not postnatal, it is similar in concept as these mice give birth on day 19.5 post-coitus, and the embryos have well developed growth plate and endochondral bone. When analyzed at P14, the E18.5–P14 S1P$^{cko\text{-}ER(T)}$ mice also demonstrated cessation of hypertrophic differentiation and loss of *Ihh*, *PTHrP-R*, and *Col10* expression in the growth plate (supplemental Fig. S4). These mice exhibited a marked chondrodysplasia (supplemental Fig. S5) not visible in P1–P7 mice (data not shown) and is more pronounced than the P1–P14 mice or mice at any other time points. Thus, the earlier the removal of S1P activity, the more severe is the resulting chondrodysplasia. Because the growth plate is disrupted, we performed TUNEL assays to test for increased apoptosis in the mutant growth plate (supplemental Fig. S6). A considerable increase in apoptosis is seen in the growth plates of S1P$^{cko\text{-}ER(T)}$ mice at all stages examined (supplemental Fig. S6, *G–L*), as compared with the WT, which showed only marginal apoptosis (supplemental Fig. S6, *A–F*). In P1–P7 mice, apoptosis is observed in both the primary growth plate (supplemental Fig. S6*G*, *arrow*) and the prospective SOC (supplemental Fig. S6, *G* and *J*). The E18.5–P14 mutant mice (which do not show any SOC development)

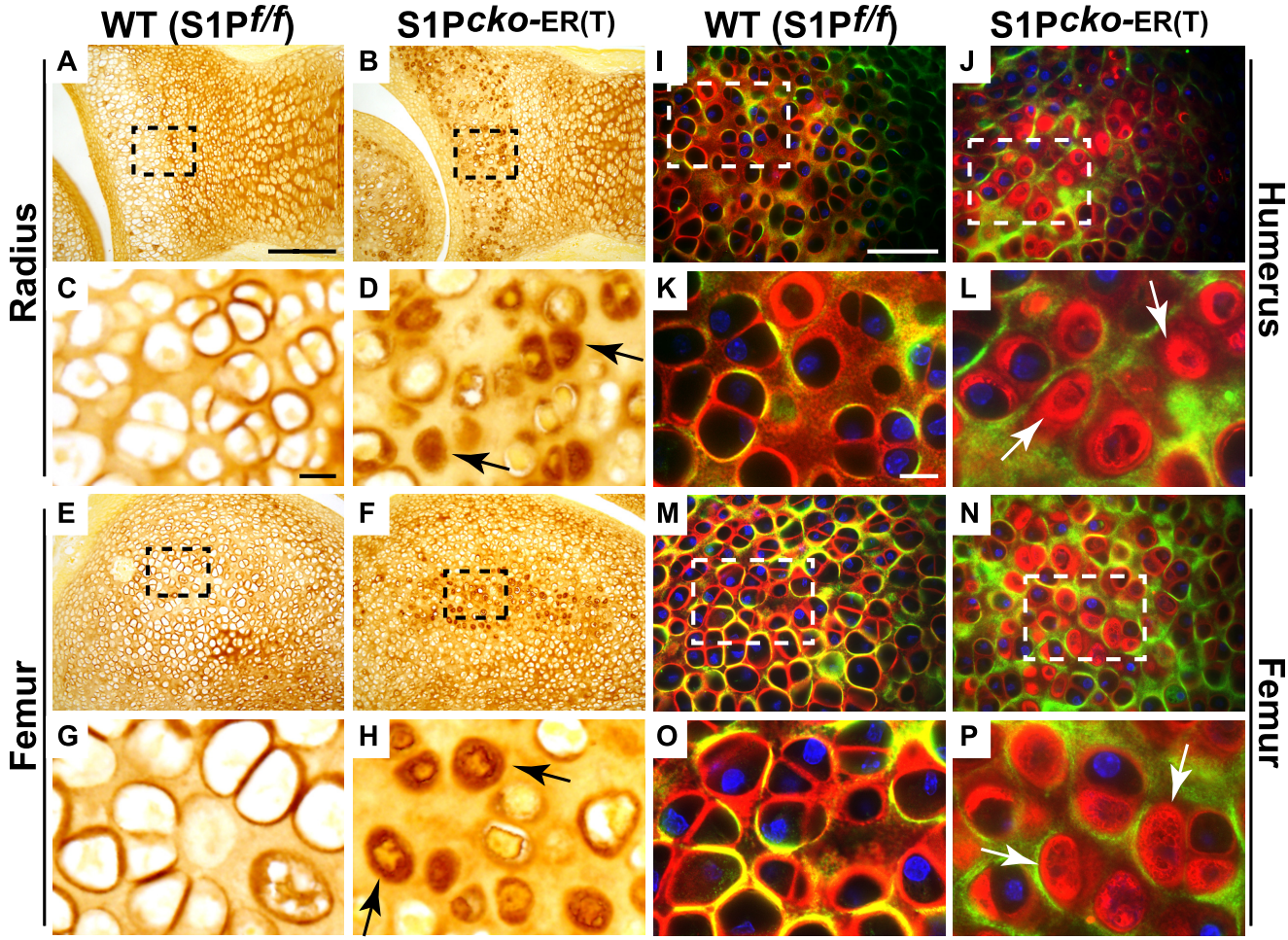

FIGURE 5. **Abnormal Col II deposition in P1-P7 S1P$^{cko\text{-}ER(T)}$ skeletal elements.** Immunohistochemistry analyses with IIF antibodies showing abnormal Col II deposition (in *brown*) in chondrocytes in the putative SOC. *C, D, G,* and *H* are higher magnification images of *A, B, E,* and *F*, respectively, with areas magnified shown *outlined*. *I–P* are double-labeled immunofluorescence studies with IIF and IIA antibodies showing abnormal Col IIB retention in chondrocytes in the prospective SOC in the mutant. *K, L, O,* and *P* are higher magnification images of *I, J, M,* and *N*. Colors representing antibody localizations are as for Fig. 3. *Arrows* in *D, H, L,* and *P* point to the abnormal Col II deposition and entrapment inside the cell. *Bars, A, B, E,* and *F,* 200 μm; *C, D, G,* and *H,* 10 μm; *I, J, M,* and *N,* 50 μm; *K, L, O,* and *P,* 10 μm.

show a more pronounced apoptosis that encompasses the entire cartilage (supplemental Fig. S6, *I* and *L*). As with the chondrodysplasia, the earlier the S1P ablation, the more pronounced the subsequent cell death.

To get mechanistic insights into the role of S1P in the postnatal growth plate, we performed a more gradual temporal analysis of S1P ablation in postnatal mice (Fig. 7). For this, we ablated S1P in S1P$^{f/f}$;Col2CreER^{T} at P1 (day 1) and analyzed the mice on day 3 (2 days later at P3), day 5 (4 days later at P5), and day 7 (6 days later at P7) to study the chronology of Col II accumulation, hypertrophy disruption, and apoptosis in the growth plate. WT (S1P$^{f/f}$) mice were studied in parallel. P1 S1P$^{f/f}$;Col2CreER^{T} mice without tamoxifen administration (Fig. 7, *A–D*) were used as controls and showed normal morphology similar to P1 WT mice (supplemental Fig. S7, *A–D*). Therefore in Fig. 7, we have compared the events in S1P$^{f/f}$;Col2CreER^{T} mice before and after S1P ablation, rather than to WT. Just 2 days since S1P ablation, P1–P3 mice demonstrated intracellular Col II retention (compare Fig. 7, *C* and *G*) that increases dramatically at P5 (Fig. 7*K*). Notably, disruption of hypertrophic differentiation proceeds in parallel to intracellular Col II retention as seen by the concomitant drop in *Col10* expression. On day 3, the S1P$^{cko\text{-}ER(T)}$ mice showed a discernible drop in *Col10* expression, although there are no morphological changes in the hypertrophic zone (compare Fig. 7, *A* with *E*). Although the WT mice also showed some decrease in *Col10* expression with maturity, the decrease is greater in the P1–P3 S1P$^{cko\text{-}ER(T)}$ mice (see supplemental Fig. S7, *F* and *H*). By P5, S1P$^{cko\text{-}ER(T)}$ mice demonstrated a sharp drop in *Col10* expression, in parallel to the dramatic increase in Col II retention (Fig. 7*K*), with a visible change in morphology (Fig. 7*I*). By day 7, in the S1P$^{cko\text{-}ER(T)}$ mice elimination of the hypertrophic zone is complete.

In sharp contrast, apoptotic events do not initiate in parallel with hypertrophic disruption and Col II retention. The beginnings of apoptosis in the growth plate in the S1P$^{cko\text{-}ER(T)}$ mice is seen only at day 5 (P1–P5 mice) and increases dramatically at day 7 (P1–P7) mice. This indicates that apoptosis is most probably a consequence of earlier events, presumably because of the intracellular Col II retention, and is likely secondary to the parallel processes of Col II retention and loss of hypertrophy. Intracellular Col II retention appears decreased in the P7 growth

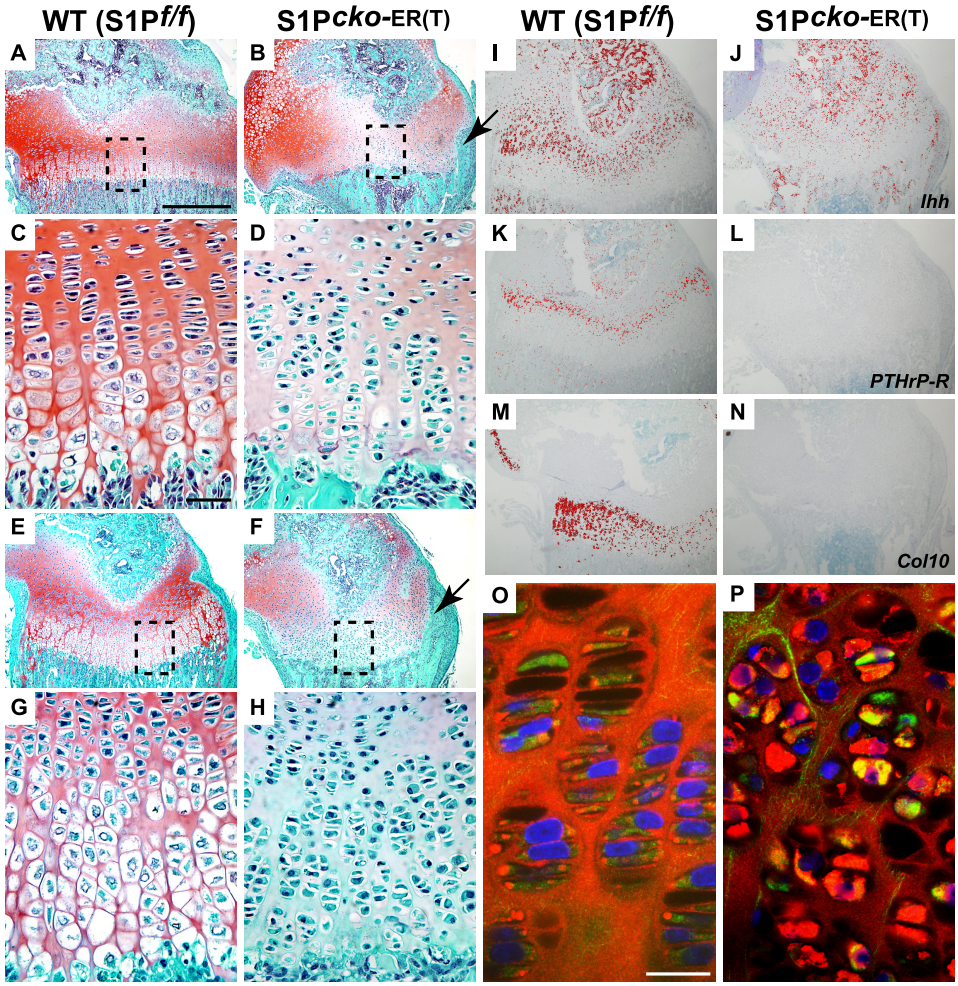

FIGURE 6. **Mutant phenotype of P7–P15 S1P$^{cko\text{-}ER(T)}$ mice due to S1P ablation at P7.** Safranin O/Fast Green-stained sections of P7–P15 WT (S1P$^{f/f}$) and S1P$^{cko\text{-}ER(T)}$ humerus (*A–D*) and femur (*E–H*) showing the elimination of hypertrophic differentiation in the mutant mice. *C, D, G,* and *H* are higher magnification images of *A, B, E,* and *F*, respectively. *Arrows* in *B* and *F* point to the bony outgrowth from the bone cortex, not seen in the WT (also see Fig. 10). *I–N* show ISH analyses in P7–P15 femurs for *Ihh* (*I* and *J*), *PTHrP-R* (*K* and *L*), and *Col10* (*M* and *N*) confirming the loss of hypertrophic cells in the mutant growth plate. *O* and *P* show double-labeled immunofluorescence studies in the femur with IIF and IIA antibodies showing abnormal Col IIB retention in the growth plate of the mutant mice. Antibody localizations are as described previously. *Bars, A, B, E, F,* and *I–N,* 500 μm; *C, D, G,* and *H,* 50 μm; *O* and *P,* 20 μm.

plate (Fig. 7*O*) that could be due to the clearing of the cells by apoptosis. Thus, these data suggest that apoptosis does not drive the phenotype in these mice. Notably, intracellular Col II retention and concomitant loss of hypertrophy appear to be related events during development.

Abnormal Bone Development in S1P$^{cko\text{-}ER(T)}$ Mice—In S1P$^{cko\text{-}ER(T)}$ mice, S1P activity is terminated after endochondral bone development is well established and yet displayed chondrodysplasia and disruption of the growth plate. To understand how this affected bone development, we performed μCT analysis of the WT and mutant femurs and humeri. P1–P7 mice, although they did not show notable differences in length between WT and mutant (see supplemental Fig. S8), showed a tremendous impact on the trabecular bone formation in the primary spongiosa (Fig. 8). In the WT, the formation of trabecular bone lamellae reflected the usual spongy nature of the bone. This was reflected both in longitudinal sections (along the long axis of the bone, Fig. 8, *A*, *C,* and *E*) and in cross-sections (axis perpendicular to the longitudinal sections) showing the metaphyseal side of the chondro-osseous junction (Fig. 8, *G* and *I*) for the distal femur or proximal humerus. Fig. 8, *K* and *M,* shows the extent of trabecular bone development and the spongy nature of the bone in a single slice of μCT scan for the WT femur or humerus, respectively. In contrast, in S1P$^{cko\text{-}ER(T)}$ mice, trabecular bone development is disrupted in both the distal femur (Fig. 8*D*) and proximal humerus (Fig. 8*F*). The bones are hollow due to loss of trabecular bone in the primary spongiosa. In cross-sections, the metaphyseal chondro-osseous junction appears sclerotic (Fig. 8, *H* and *J*); the entire metaphyseal region appears as a dense mass of fused lamellae, also reflected in images of individual μCT slices (*arrow* in Fig. 8, *L* and *N*). The disruption in trabecular bone development is not simply a delay but is also seen in P1–P14 S1P$^{cko\text{-}ER(T)}$ mice (supplemental Fig. S9, *B* and *D*). As the animals aged, differences in size and in their bones, between WT and mutant mice, become significant and more visible (supplemental Figs. S5 and S8).

To understand trabecular bone disruption further in the S1P$^{cko\text{-}ER(T)}$ mice, we analyzed the μCT scans of P1–P7 femurs slice by slice, with and without segmentation, in cross-sections of the bones starting from the metaphyseal side of the chondro-osseous junction of the distal femur and progressing toward the diaphysis (Fig. 9). In the WT, trabecular bone develops uni-

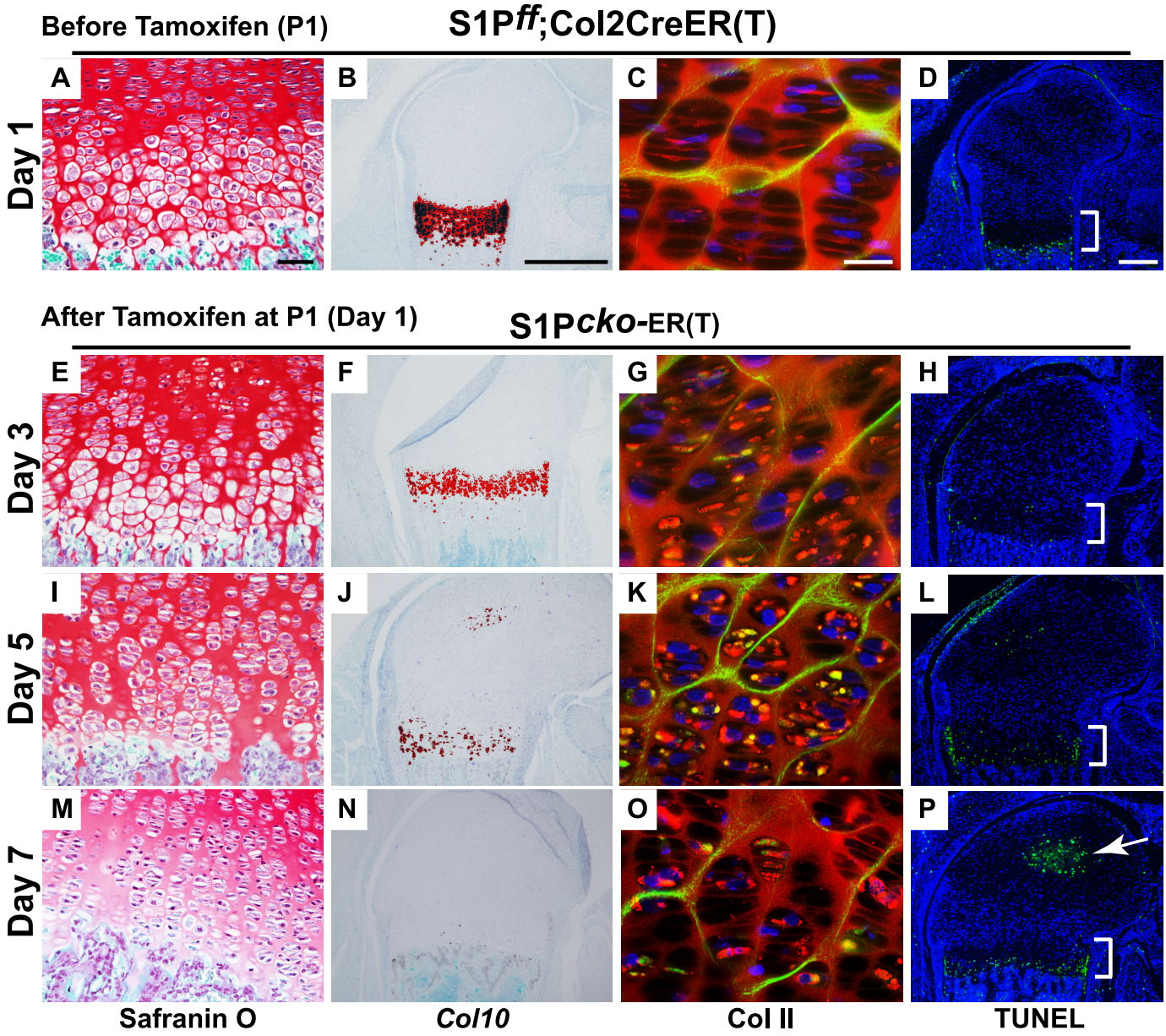

FIGURE 7. **Chronology of intracellular Col II retention, loss of hypertrophy, and apoptosis after S1P ablation.** WT (S1P$^{f/f}$) (also see supplemental Fig. S7) and S1P$^{f/f}$;Col2CreER^{T} mice were injected with tamoxifen at P1 (day 1), and the distal end of femur was analyzed on days 3 (*E–H*), 5 (*I–L*), and 7 (*M–P*) by Safranin O staining, *Col10* ISH, double-labeled immunofluorescence with IIF and IIA antibodies for Col II deposition, and by TUNEL assays to analyze the sequence of events. As the S1P$^{f/f}$;Col2CreER^{T} mice show no abnormality and are equivalent to WT (S1P$^{f/f}$) mice before S1P ablation, comparisons in this figure are shown only for the S1P$^{f/f}$;Col2CreER^{T} mice before and after (S1P$^{cko\text{-}ER(T)}$) S1P ablation. The growth plate is demarcated by a *bracket* in the TUNEL assays, and the *arrow* in *P* points to apoptosis in the SOC. *Bars, A, E, I,* and *M,* 50 μm; *B, F, J,* and *N,* 500 μm; *C, G, K,* and *O,* 20 μm; *D, H, L,* and *P,* 200 μm.

formly and gradually from one slice to the next, over the entire area of the metaphysis, and the spongy nature of the bone is apparent. It is barely possible to distinguish the compact and dense bone collar from the trabecular bone. In contrast, in P1–P7 S1P$^{cko\text{-}ER(T)}$ mice, the trabecular bone development is seen as a dense mass in the center of the metaphysis surrounded by the easily discernible compact bone collar. The change in metaphyseal bone development from one slice to the next is not gradual but abrupt, and bone development takes place in a couple of random directions toward the bone collar rather than uniformly in all directions. The trabecular bone is not spongy and appears as a dense sclerotic mass of trabecular lamellae.

Similarly, we analyzed the morphology of the femurs (and humeri; data not shown) when S1P was ablated in the P7 mice. As the animals aged, the difference in length of the femurs with the WT becomes more dramatic and heightens the resulting chondrodysplasia in S1P$^{cko\text{-}ER(T)}$ mice (supplemental Figs. S5 and S8). Even as early as P15, the trabecular bone in the primary spongiosa is dramatically diminished as seen in longitudinal sections (Fig. 10*G*). In cross-sections, the metaphyseal chondro-osseous junction in the distal femur does not appear spongy (Fig. 10*J*) as in the WT (Fig. 10*D*). The overall morphology of these mutant bones is similar to that seen in the P1–P7 mutant mice. With age, the S1P$^{cko\text{-}ER(T)}$ mice are unable to remedy trabecular bone disruption. The primary spongiosa is dras-

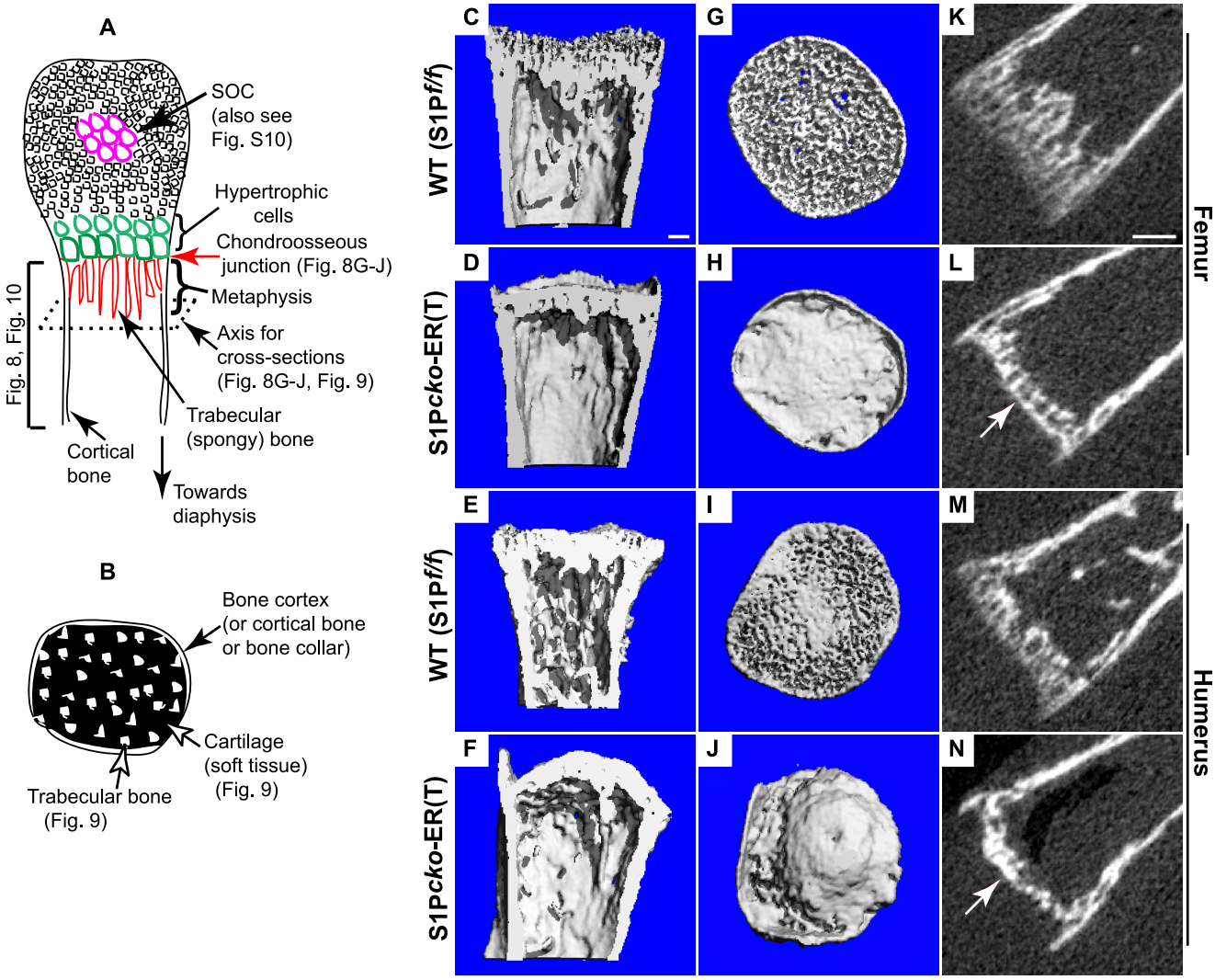

FIGURE 8. **Morphology of the humerus (proximal) and femur (distal) in P1–P7 WT (S1P$^{f/f}$) and S1P$^{cko\text{-}ER(T)}$ mice as imaged by μCT showing the loss of trabecular lamellae and the sclerotic nature of the mutant metaphysis.** *A* and *B* are schematics as an aid to understand the orientation of the μCT images in Figs. 8–10. *A* shows a longitudinal section (along the long axis) through the center of a bone imaged in *C–F* and *K–N*. The bone in cross-sections, at an angle perpendicular to the longitudinal axis (axis for cross-section), is imaged in *G–J* (and in Fig. 9). The *red arrow* points to the chondro-osseous junction imaged in *G–J* on the metaphyseal side. *B* is a schematic particularly applicable to Fig. 9 showing the metaphysis/trabecular bone development in a cross-section. Although *C–J* are reconstructed bone images from μCT scans, *K–N* are images of a single μCT scan slice showing the diminished spongy bone formation in S1P$^{cko\text{-}ER(T)}$ mice. The *arrow* in *L* and *N* point to the sclerotic dense nature of the metaphyseal side of the chondro-osseous junction in the mutant mice. *Bars, C–J,* 100 μm; *K–N,* 250 μm.

tically diminished, and the last remnants of trabecular bone seen in P7–P15 S1P$^{cko\text{-}ER(T)}$ mice is totally lost in P7–P28 or P7–P42 S1P$^{cko\text{-}ER(T)}$ mice (Fig. 10, *H* and *I*). As S1P$^{f/f}$; Col2CreER^{T} mice show well formed and normal trabecular bone at P10 and later (supplemental Fig. S9, *E–H*) in the primary spongiosa in the absence of S1P ablation by tamoxifen, these data indicate the requirement of S1P for normal trabecular bone development, presumably through growth plate maintenance. On S1P ablation, the well formed trabecular bone is almost completely decimated.

In P7–P15 mice, the perichondrial tissue at one edge of the growth plate is replaced by bone cortex in the mutant (*arrowheads*, Fig. 10*N*; also Fig. 6, *B* and *F*) that are extensions from the cortical bone and are responsible for the bony protrusions in the μCT images (*arrows,* Fig. 10, *G* and *J*). This development appears to be analogous to the enhanced cortical bone seen in E10.5 (or E13.5)-E18.5 S1P$^{cko\text{-}ER(T)}$ mice and in the S1P^{cko} mice.

In WT mice as the growth plate matures, undulations in the growth plate result in the formation of four mammillary processes (15) in the metaphyseal chondro-osseous junction shown in P7–P28 and P7–P42 WT mice (*asterisks,* Fig. 10). The termination of S1P activity in S1P$^{cko\text{-}ER(T)}$ mice and the consequent chondrocyte apoptosis prevent growth plate maturation and undulations, and this is mirrored by a lack of development of the mammillary processes in the metaphyseal chondro-osseous junction in the mutants (Fig. 10, *H, I, K,* and *L*). Taken together with the chondrodysplasia, these data suggest an inactive, dead, growth plate in the mutant mice. But remarkably, these mice develop an additional, fully functional growth plate, the beginnings of which can be seen in E18.5–P14 S1P$^{cko\text{-}ER(T)}$ mice (supplemental Fig. S4). In P7–P28 mutant mice, the development of this new growth plate (Fig. 10, *P* and *R*) results in the SOC being pushed to one side (Fig. 10, *H* (*arrow*) and *P*), whereas the primary growth plate is gradu-

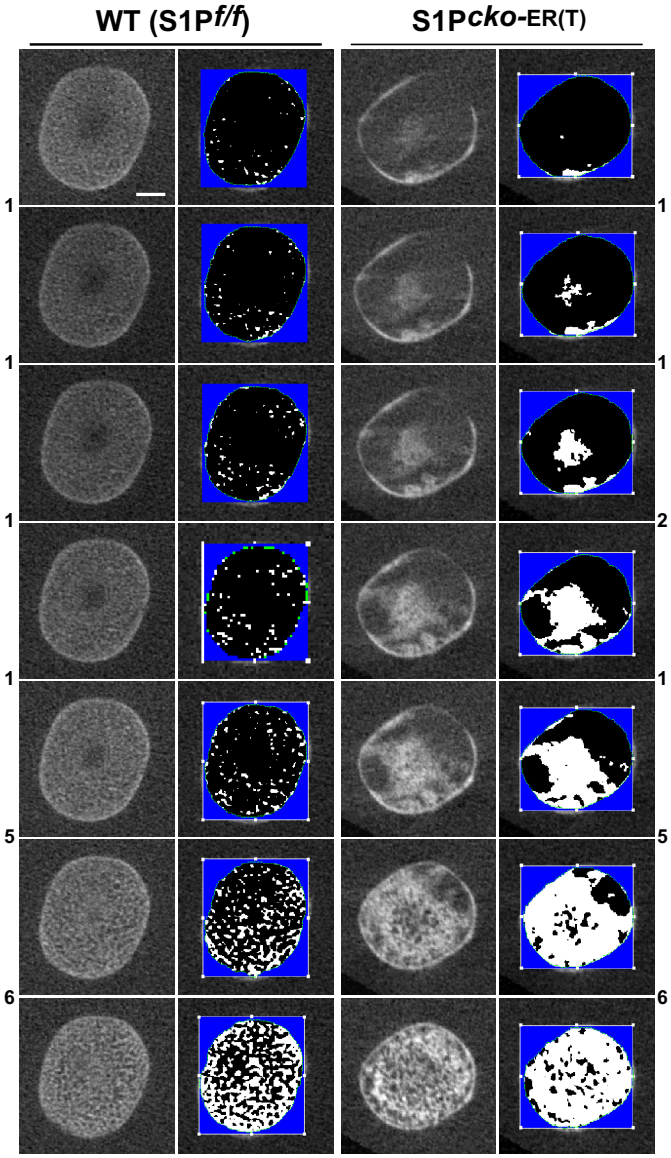

FIGURE 9. **Femoral trabecular bone development in P1–P7 S1P$^{cko\text{-}ER(T)}$ mice.** Figure shows images of individual scan slices from μCT at intervals, and their corresponding segmentation slices (against a *blue* background) to distinguish soft tissue such as cartilage (in *black*) from bone (in *white*), in cross-sections (see Fig. 8*B*) of the distal femur, demonstrating the abnormal profile of the mutant trabecular bone. The *number* between the panels refers to the number of μCT scan slice(s) skipped in-between, with those for WT shown on the *left* and for the mutant on the *right*. *Bar*, (*all panels*) 0.25 mm.

ally eradicated (*arrow*, Fig. 10*R*) and is almost nonexistent in P7–P42 mutant mice. In the latter, this new growth plate has developed enough to support the growth of new trabecular bone (*arrowheads*, Fig. 10, *I*, *L*, and *T*) that is now aligned with the cortical bone formed from the primary growth plate prior to S1P ablation (*arrow*, Fig. 10, *I* and *T*), because of the bending of the distal femur. Fig. 10 also demonstrates that with time the width of the mutant bones become smaller compared with WT; this is most evident in the P7–P42 mice where the mutant femur is less than 1 mm (~750 μm) wide, whereas the WT femur is about 1.5 mm.

To understand the nature of the residual trabecular bone in S1P$^{cko\text{-}ER(T)}$ mice, we performed histomorphometric measurements from the μCT scans (Table 2 and supplemental Table 1). At each developmental stage, S1P$^{cko\text{-}ER(T)}$ mice exhibit higher BV/TV and higher BMD than the WT trabecular bone that would explain the dense, sclerotic appearance of the mutant trabecular bones seen in the μCT images. SOC development is also affected in post-P7 ablated mutant mice and reflects the lack of development of the mammillary processes in these mice (supplemental Fig. S10). The activity of osteoclasts appear normal as the mutant mice show tartrate-resistant acid phosphatase staining in the trabecular bone of the metaphysis and in the SOC, similar to the WT (supplemental Fig. S11). Normal osteoblast activity is also suggested by the incorporation of both calcein and alizarin-red dyes into newly deposited bone cortex or SOC (supplemental Fig. S12).

DISCUSSION

In this study, we have demonstrated a critical role for S1P in preserving the postnatal growth plate that is fundamental to long bone growth through endochondral bone development in postnatal mice. Preservation of the growth plate appears to be related to chondrocyte maturation via hypertrophic differentiation as S1P ablation in postnatal chondrocytes eliminates hypertrophic differentiation as evidenced from the absence of *Ihh*, *PTHrP-R*, and *Col10* expression in the growth plate. The absence of *Ihh* and *PTHrP-R* expression in the growth plate accentuates a total termination of chondrocyte differentiation as these genes are expressed in the pre-hypertrophic cells. Intracellular Col II accumulation is almost immediate and is concomitant with loss of hypertrophy suggesting that these two processes might be regulated in tandem. S1P is also a critical regulator of SOC development as in its absence SOC development was prematurely aborted. Besides the impediment to bone elongation, disruption of the growth plate also reduced bone width and decimated trabecular bone in the primary spongiosa with the residual metaphyseal region appearing dense and sclerotic, presumably because of the higher BMD and BV/TV. Table 1 summarizes some of the phenotypic manifestations of S1P ablations in prenatal and postnatal mice.

The absence of Ihh expression in the growth plate on postnatal S1P ablations might suggest that the mutant phenotypes seen in these mice are due to the loss of Ihh in the growth plate. S1P could indeed indirectly affect Ihh functions because of its role in lipid homeostasis and the necessary lipophilic Ihh modifications required to establish a gradient of Ihh activity thought to be critical for its function (16, 17). Ihh has also been shown to govern, directly or indirectly, various aspects of endochondral bone formation in mice (12, 18–20). However, a number of fundamentally different phenotypes in Ihh and S1P knock-out mice indicate that abnormal Ihh activity is not causal to the phenotype seen on S1P ablation. Postnatal ablation of Ihh results in mice with a complete loss of the rounded articular surface, loss of columnar structure of chondrocytes, a growth plate composed primarily of hypertrophic chondrocytes that expressed *PTHrP-R* and *Col10*, and the presence of viable chondrocytes in the growth plate as evidenced by lack of apoptosis by TUNEL staining (21). However, S1P$^{cko\text{-}ER(T)}$ mice contradict these very phenotypes and are exactly the opposite of postnatal Ihh knock-out mice indicating that the phenotypes observed in S1P$^{cko\text{-}ER(T)}$ mice are primarily due to the loss of loss of S1P

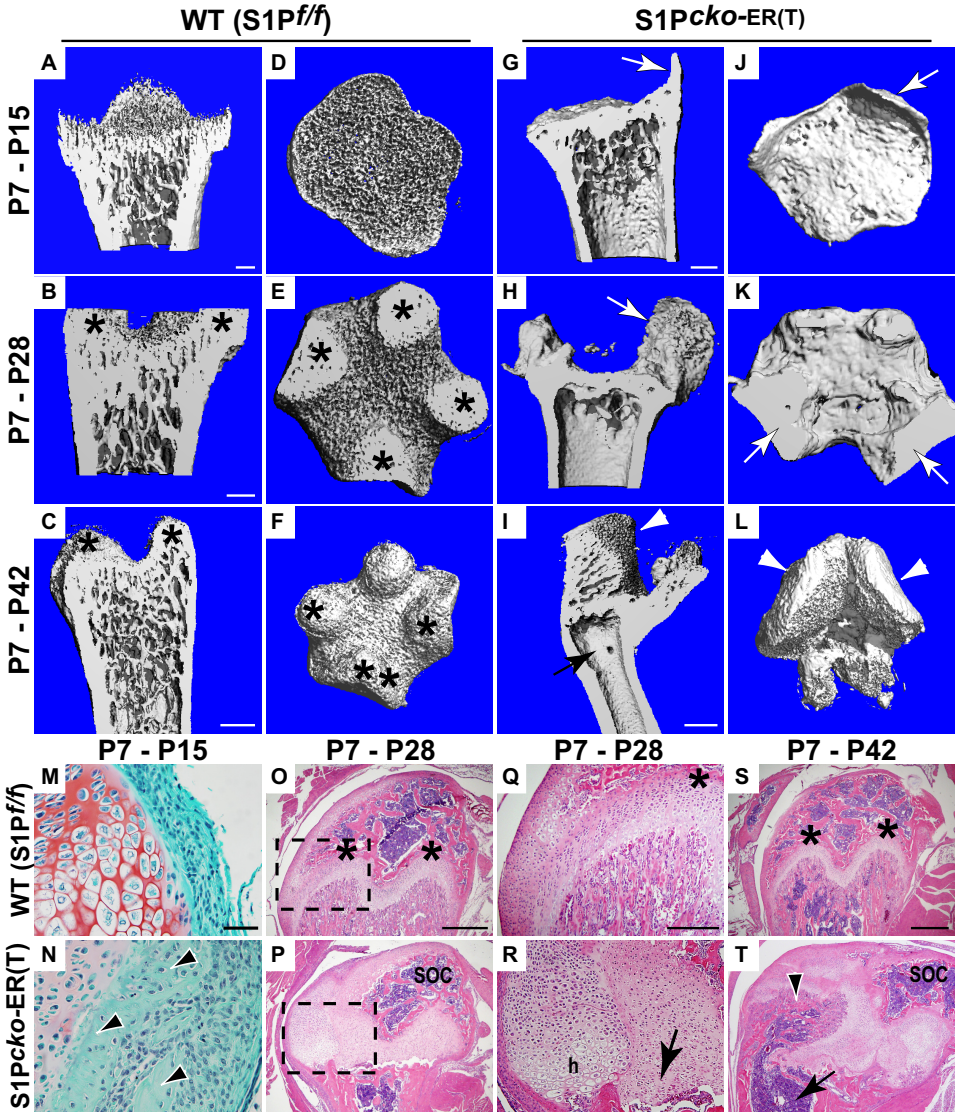

FIGURE 10. **Nature of the bone on S1P ablation at P7.** Femurs from WT (S1P$^{f/f}$) and S1P$^{cko\text{-}ER(T)}$ mice with S1P ablation at P7 were harvested at P15, P28, and P42 and analyzed by μCT. Images of longitudinal sections through the center (*A–C* and *G–I*) or of cross-sections at the metaphyseal side of the chondro-osseous junction (*D–F* and *J–L*), from reconstructed μCT scans of distal femurs, show the sclerotic nature of the metaphyseal chondro-osseous junction and the decimated trabecular bone in the mutant mice (*G–L*), as compared with WT (*A–F*). *M* and *N* are Safranin O/Fast Green-stained sections showing the extensions from the bone cortex (*arrowheads* in *N*; *arrows* in *G* and *J*) replacing the perichondrial tissue at the edge of the growth plate in the mutant. *O–T* are H&E-stained sections showing bone morphology with *Q* and *R* being higher magnification images of regions *outlined* in *O* and *P*. *Asterisks* in *B, C, E, F, O, Q,* and *S* mark the mammillary processes formed in the metaphyseal chondro-osseous junction in the WT because of undulations in the maturing growth plate. *Arrows* in *H* and *K* point to the SOC (also see *P*) that is pushed aside to accommodate the additional growth plate shown in P7–P28 mutants (*P*) with normal hypertrophic (*h*) cells (*R*). The *arrow* in *R* points to the dead, inactive primary growth plate. In the older P7–P42 mutant mice, this new growth plate allows for development of new trabecular bone (*arrowheads* in *I, L,* and *T*), which is now aligned with the cortical bone (*arrow* in *I* and *T*) due to bending of the distal femur. *Bars, A* and *D,* 200 μm; *G* and *J,* 200 μm; *B, E, H,* and *K,* 200 μm; *C* and *F,* 500 μm; *I* and *L,* 500 μm; *M* and *N,* 50 μm; *O* and *P,* 500 μm; *Q* and *R,* 250 μm; *S* and *T,* 500 μm.

activity and not related to the loss of *Ihh* expression. The phenotype in S1P$^{cko\text{-}ER(T)}$ mice is neither due to the loss of PTHrP-R expression as postnatal loss of PTHrP-R demonstrates accelerated chondrocyte differentiation (22) as opposed to the loss of differentiation seen on postnatal S1P ablation.

In S1P^{cko} mice (8), endochondral bone formation was completely prevented even though the molecular program for endochondral bone development appeared intact. S1P appeared to have a role in the development of normal cartilage matrix via a role in Col IIB deposition. As S1P ablations at E10.5 also result in loss of endochondral bone formation, the mechanism preventing endochondral bone formation would be similar to S1P^{cko} mice as the molecular program required for endochondral bone formation is also intact in E10.5–E18.5 S1P$^{cko\text{-}ER(T)}$ mice. In these mice, although areas of normal collagen deposition are seen (Fig. 3, *E* and *H*), the cartilage matrix is mostly irregular, and abnormal Col IIB retention within the cells (Fig. 3, *B, C, F,* and *I*) is observed coinciding with a predominance of Col IIA in the matrix. In S1P^{cko} mice, the Col II-hypomorphic defective cartilage matrix presumably made it difficult for vascular invasion and for the entry of osteoblastic precursors to seed endochondral bone. Besides chondrocytes, Col2Cre lines also target S1P-expressing perichondrial cells from where the osteoblastic precursors invade the matrix. Thus, one may hypothesize that a lack of S1P activity in these perichondrial osteoblastic progenitors could prevent endochondral bone

TABLE 2

Histomorphometric measurements of BV/TV and BMD in WT ($S1P^{f/f}$) and $S1P^{cko\text{-}ER(T)}$ mice

Histomorphometric measurements of BV/TV and BMD (expressed as milligrams of hydroxyapatite (HA)/cm^3) were done on the distal femur or proximal humerus using 50 μCT scan slices beginning from the metaphyseal side of the chondro-osseous junction ($n = 3$ at each stage). The p value for BV/TV comparisons is <0.01, except for P1–P7 humerus where it is not significant; the p value for BMD comparisons is <0.05, except for P1–P7 humerus where it is not significant; however, the p value for the entire WT *versus* mutant comparison in this table is <0.05. All measurements shown are for the primary spongiosa. WT = wild type ($S1P^{f/f}$); CKO = $S1P^{cko\text{-}ER(T)}$.

		BV/TV		BMD (mg of HA/cm^3)	
Phenotype	Bone	WT	CKO	WT	CKO
P1–P7	Femur	0.445333 ± 0.011	0.5095 ± 0.005	260.6517 ± 7.076	274.3818 ± 8.097
	Humerus	0.6137 ± 0.104	0.593467 ± 0.022	301.7787 ± 35.79	328.5415 ± 18.29
P7–P15	Femur	0.258433 ± 0.074	0.692333 ± 0.113	217.0186 ± 25.16	393.5931 ± 66.23
	Humerus	0.444767 ± 0.078	0.694267 ± 0.077	262.568 ± 17.95	397.0888 ± 45.11

development. But removal of S1P does not ablate normal osteoblastogenesis as extrapolated from the formation of the enhanced bone cortex in E10.5–E18.5 and E13.5–E18.5 $S1P^{cko\text{-}ER(T)}$ mice as well as the extension of bone cortex seen in P7–P15 mutant mice (Figs. 6, *B* and *F*, and 10*N*). Also, lineage tracing experiments with $Col2CreER^T$ mice demonstrated that although chondrocytes contribute to osteoblastic progenitors, these are largely restricted to the cartilage-perichondrial interface and to the endosteum; osteoblasts of the primary spongiosa are derived primarily from osterix-expressing cells (not *Col2a1*-expressing cells) and therefore should be unaffected by the Col2Cre activity (23). These observations reinforce the causal nature of the defective matrix in preventing endochondral bone formation in early embryonic, prenatal S1P ablations.

E10.5–E18.5 and E13.5–E18.5 $S1P^{cko\text{-}ER(T)}$ mice display an additional phenotype not seen in $S1P^{cko}$ mice, namely the lack of Col IIB integrity in the matrix as interpreted from the polygonal or ring-like Col IIB structures mostly seen in the hypertrophic matrix (Fig. 3*N* and supplemental Fig. S3, *F* and *L*). On S1P ablation, the secreted Col IIB appears unable to maintain its integrity in the matrix in the absence of peak levels of S1P activity. This could arise from a lack of sufficient Col IIB processing, directly or indirectly via S1P, the exact nature of which awaits characterization. Moreover, the immature endochondral bone formation coupled with enhanced cortical bone formation and lethality in E13.5–E18.5 $S1P^{cko\text{-}ER(T)}$ mice indicates a continuous requirement for S1P during embryonic endochondral bone development.

Our studies with postnatal S1P ablations indicate more than a casual link between S1P, Col IIB deposition, and hypertrophy. Our time course experiments with P1–P7 mice indicate an almost immediate Col IIB entrapment in the chondrocytes with concomitant loss of chondrocyte hypertrophy in the primary growth plate suggesting a link between these two diverse and distinct developmental pathways. Although the nature of this convergence remains to be explored, at the very least these observations suggest that continuous, normal secretion or processing of Col IIB is required for normal hypertrophy. It is also possible that due to the increasing entrapment of Col IIB with time, and the consequent disruption of the native pericellular matrix, chondrocyte-matrix interactions are disrupted, and signaling mechanisms required for chondrocyte hypertrophy are disrupted. Thus, the faulty Col IIB deposition could still be the primary reason for the phenotypes that indicate a direct or indirect role for S1P in Col IIB processing. As to how and why they manifest phenotypically differently in pre- and postnatal mice, however, remains to be studied. Abnormal retention of Col IIB is also observed within the prospective SOC precluding its development. This observation underscores the importance of normal Col IIB deposition for SOC development as well. Unlike the $S1P^{cko}$ mice where, despite *Ihh*, *PTHrP-R*, and *Col10* expression, the cells did not form an organized growth plate structure, in postnatal mice the arrangement of cells is not random, and the columnar arrangement of chondrocytes in the growth plate is as in the WT. It appears therefore that once the last of the hypertrophic cells is excavated, no further hypertrophic differentiation could take place, thereby eliminating growth plate functions and impeding further bone elongation.

A common phenotype seen in all S1P-knock-out mouse models, whether prenatal or postnatal, is the induction of apoptosis. Extensive chondrocyte apoptosis is seen in both the primary growth plate and in cells of the putative SOC. Our time course studies clearly demonstrate that apoptosis is not immediate and is therefore ancillary to the concomitant processes of intracellular Col IIB retention and disruption of hypertrophic differentiation. Mechanistically, this is indicative of the perturbation of developmental pathways different from that regulated by other growth plate molecules such as PTHrP-R whose postnatal ablation is characterized by apoptotic events fundamental to growth plate closure (22). Although the growth plate in $S1P^{cko\text{-}ER(T)}$ is rendered inactive due to loss of hypertrophy, with time it is also rendered nonexistent due to apoptotic activity. As the primary growth plate is gradually eradicated, an additional normal growth plate takes its place, complete with normally developing trabecular bone. Thus, our study demonstrates that additional source(s) of progenitor stem cells are capable of regenerating the growth plate. We are not sure about the provenance of these progenitors. The perichondrium (24) or the periosteum (25) is a probable source of these progenitors. It is also likely that bone marrow stromal cells are able to colonize a suitable niche within the dying growth plate and colonize the area to initiate a new growth plate (26). The progenitors can access this niche within the dying growth plate by using the metaphyseal blood vessels, or the ring vessel, or the subperichondrial plexus, depending on their origin or the route taken (27). Thus, our studies suggest the possibility of artificially rejuvenating growth plates to correct bone defects arising from mutational events.

The anomalous trabecular bone defect seen in postnatal mice appears secondary to S1P knock-out and is probably an after effect of growth plate obliteration and is due to the lack of further contribution of chondrocytes to the endochondral bone developmental program. Although S1P is also expressed in the perichondrium, a faulty perichondrium is unlikely to be the cause of the abnormal bone phenotype as the ability of Col2Cre mice to target the perichondrium progenitors is lost very early around E13.5, at which time only the chondrocytes in the cartilage appear to have strong Cre activity (9, 23, 28). Furthermore, the activity of the osteoclasts and osteoblasts in bone formation appears intact in these mice, judging from the normal tartrate-resistant acid phosphatase staining and the incorporation of calcein/alizarin-red dyes into bone cortex or SOC. The constant remodeling activity of the osteoblasts and osteoclasts on the trabecular bone in the primary spongiosa formed before S1P ablation, in the absence of any further bone elongation, presumably depletes the residual metaphyseal region resulting in loss of trabecular bone architecture. This in turn leads to higher bone mineral density and bone volume fraction as bone deposition is now taking place in the absence of bone elongation. These observations thus endorse the importance of S1P in coupling growth plate development to trabecular bone development. This is important in light of the fact that not all ablations of growth plate molecules lead to diminished trabecular bone as seen in the case of Schnurri-2 and Schnurri-3 where knock-out of these growth plate molecules in mice impaired growth plate maturation but enhanced trabecular bone formation (29).

In summary, our study demonstrated that S1P plays important roles in growth plate maintenance and bone development in postnatal mice. Given its role as a proprotein convertase, S1P may affect these functions via the processing of biological effectors such as ATF6 or sterol regulatory element-binding proteins, which is under further investigation in the laboratory. Our study accentuates a critical need for S1P in skeletal homeostasis as it couples cartilage development to trabecular bone development in the primary spongiosa during long bone elongation through endochondral ossification.

Acknowledgments—We thank Susan Mackem (Center for Cancer Research, NCI, National Institutes of Health) for the gift of Col2CreER^T mice. We thank Jennifer Bryan for technical assistance in some experiments. We thank Cornelia Farnum (Cornell University) and Jeffrey Gorski (University of Missouri, Kansas City) for their critical reading of the manuscript and helpful suggestions. We thank Crystal Idleburg of the Molecular Analysis subdivision of Washington University Center for Musculoskeletal Research for assistance with histological analysis and Tarpit Patel of the Musculoskeletal Structure and Strength Core subdivision of the Center for Musculoskeletal Research for assistance with MicroCT studies.

REFERENCES

1. Brown, M. S., Ye, J., Rawson, R. B., and Goldstein, J. L. (2000) *Cell* **100,** 391–398
2. Eberlé, D., Hegarty, B., Bossard, P., Ferré, P., and Foufelle, F. (2004) *Biochimie* **86,** 839–848
3. Ye, J., Rawson, R. B., Komuro, R., Chen, X., Davé, U. P., Prywes, R., Brown, M. S., and Goldstein, J. L. (2000) *Mol. Cell* **6,** 1355–1364
4. Murakami, T., Kondo, S., Ogata, M., Kanemoto, S., Saito, A., Wanaka, A., and Imaizumi, K. (2006) *J. Neurochem.* **96,** 1090–1100
5. Zhang, K., Shen, X., Wu, J., Sakaki, K., Saunders, T., Rutkowski, D. T., Back, S. H., and Kaufman, R. J. (2006) *Cell* **124,** 587–599
6. Provot, S., and Schipani, E. (2005) *Biochem. Biophys. Res. Commun.* **328,** 658–665
7. Schlombs, K., Wagner, T., and Scheel, J. (2003) *Proc. Natl. Acad. Sci. U.S.A.* **100,** 14024–14029
8. Patra, D., Xing, X., Davies, S., Bryan, J., Franz, C., Hunziker, E. B., and Sandell, L. J. (2007) *J. Cell Biol.* **179,** 687–700
9. Nakamura, E., Nguyen, M. T., and Mackem, S. (2006) *Dev. Dyn.* **235,** 2603–2612
10. Yang, J., Goldstein, J. L., Hammer, R. E., Moon, Y. A., Brown, M. S., and Horton, J. D. (2001) *Proc. Natl. Acad. Sci. U.S.A.* **98,** 13607–13612
11. Hildebrand, T., Laib, A., Müller, R., Dequeker, J., and Rüegsegger, P. (1999) *J. Bone Miner. Res.* **14,** 1167–1174
12. Long, F., Zhang, X. M., Karp, S., Yang, Y., and McMahon, A. P. (2001) *Development* **128,** 5099–5108
13. Zhu, Y., Oganesian, A., Keene, D. R., and Sandell, L. J. (1999) *J. Cell Biol.* **144,** 1069–1080
14. Baron, R., Vignery, A., Neff, L., Silvergate, A., and Santa Maria, A. (1983) in *Bone Histomorphometry: Techniques and Interpretation* (Recker, R. R., ed) pp. 13–35, CRC Press, Inc., Boca Raton, FL
15. Lerner, A. L., and Kuhn, J. L. (1997) *J. Orthop. Res.* **15,** 353–361
16. Gritli-Linde, A., Lewis, P., McMahon, A. P., and Linde, A. (2001) *Dev. Biol.* **236,** 364–386
17. Koziel, L., Kunath, M., Kelly, O. G., and Vortkamp, A. (2004) *Dev. Cell* **6,** 801–813
18. Joeng, K. S., and Long, F. (2009) *Development* **136,** 4177–4185
19. Long, F., Chung, U. I., Ohba, S., McMahon, J., Kronenberg, H. M., and McMahon, A. P. (2004) *Development* **131,** 1309–1318
20. St-Jacques, B., Hammerschmidt, M., and McMahon, A. P. (1999) *Genes Dev.* **13,** 2072–2086
21. Maeda, Y., Nakamura, E., Nguyen, M. T., Suva, L. J., Swain, F. L., Razzaque, M. S., Mackem, S., and Lanske, B. (2007) *Proc. Natl. Acad. Sci. U.S.A.* **104,** 6382–6387
22. Hirai, T., Chagin, A. S., Kobayashi, T., Mackem, S., and Kronenberg, H. M. (2011) *Proc. Natl. Acad. Sci. U.S.A.* **108,** 191–196
23. Maes, C., Kobayashi, T., Selig, M. K., Torrekens, S., Roth, S. I., Mackem, S., Carmeliet, G., and Kronenberg, H. M. (2010) *Dev. Cell* **19,** 329–344
24. Togo, T., Utani, A., Naitoh, M., Ohta, M., Tsuji, Y., Morikawa, N., Nakamura, M., and Suzuki, S. (2006) *Lab. Invest.* **86,** 445–457
25. Xie, C., Ming, X., Wang, Q., Schwarz, E. M., Guldberg, R. E., O'Keefe, R. J., and Zhang, X. (2008) *Bone* **43,** 1075–1083
26. Liu, X., Sun, H., Yan, D., Zhang, L., Lv, X., Liu, T., Zhang, W., Liu, W., Cao, Y., and Zhou, G. (2010) *Biomaterials* **31,** 9406–9414
27. Farnum, C. E., Lenox, M., Zipfel, W., Horton, W., and Williams, R. (2006) *Anat. Rec. A Discov. Mol. Cell Evol. Biol.* **288,** 91–103
28. Hilton, M. J., Tu, X., and Long, F. (2007) *Dev. Biol.* **308,** 93–105
29. Jones, D. C., Schweitzer, M. N., Wein, M., Sigrist, K., Takagi, T., Ishii, S., and Glimcher, L. H. (2010) *Proc. Natl. Acad. Sci. U.S.A.* **107,** 8254–8258